Journal of Energy Chemistry 41 (2020) 93–99

Contents lists available at ScienceDirect

Journal of Energy Chemistry

journal homepage: www.elsevier.com/locate/jechem

http://www.journals.elsevier.com/journal-of-energy-chemistry/

The effect of Al^{3+} coordination structure on the propane dehydrogenation activity of $Pt/Ga/Al_2O_3$ catalysts

Qinqin Yu, Tie Yu*, Hongyu Chen, Guangzong Fang, Xiulian Pan, Xinhe Bao

State Key Laboratory of Catalysis, Dalian Institute of Chemical Physics, Chinese Academy of Sciences, Dalian 116023, Liaoning, China

ARTICLE INFO

Article history:
Received 20 March 2019
Revised 23 April 2019
Accepted 26 April 2019
Available online 11 May 2019

Keywords:
Dehydrogenation
Ga_2O_3
Al_2O_3
Coordinatively unsaturated

ABSTRACT

The effect of the Al_2O_3 structure on the performance of $Pt/Ga/Al_2O_3$ catalysts is investigated for the direct dehydrogenation of propane. The study unveils that the structure of Al^{3+} determines the bulk structure of catalysts, particularly a high content of coordinatively unsaturated Al^{3+} sites (penta-coordinated Al^{3+}, denoted as Al^{3+}_{penta}) could lead to a remarkably improved dehydrogenation activity of the catalyst. The bulk characterization reveals that the sufficient amount of Al^{3+}_{penta} in Al_2O_3 benefit the dispersion of Pt and Ga_2O_3 on the Al_2O_3 support. At the same time, TPR results reveal that the presence of Pt facilitates the reduction of Ga_2O_3, likely due to the hydrogen spillover between the well dispersed Pt and Ga_2O_3, which consequently enhances the synergistic function between Pt and Ga_2O_3 in the dehydrogenation of propane. Recyclability tests demonstrate that the dehydrogenation activity stabilizes after three cycles over the $Pt/Ga/Al_2O_3$ catalyst.

1. Introduction

The catalytic dehydrogenation of propane (PDH) is one of the most important issues in chemical engineering industry due to the growing demand for propylene throughout the world. Moreover, the on-going shale gas exploration imposes significant technical and economic challenges and opportunities for the traditional petrochemical industry. Under such a background, production of light alkenes from alkanes gains renewed attention [1] not only in academia but also in chemical industry. It is known that PtSn (Oleflex process from UOP) [2–4] and CrO_x (Catofin process from CB&I Lummus) [5–7] supported on Al_2O_3 are active catalysts for the dehydrogenation of light alkanes, and have been widely employed in commercial dehydrogenation processes. Although substantial understanding of the catalytic mechanism has been gained and consequently catalytic performance improved, the limited resource of Pt and the environmental pollution from Cr still demand the search for alternative economic and eco-friendly catalysts.

Ga_2O_3 is another typical non-precious metal oxide for dehydrogenation of light alkanes and has been investigated intensively. Both bulk and supported Ga_2O_3 have been utilized as catalysts for the dehydrogenation of propane to propylene, and Ga_2O_3 supported on alumina seems the most common one among these catalysts [8–10]. A heterolytic dissociation reaction mechanism was proposed and the Lewis acid sites generated on the catalysts through the interaction of Ga_2O_3 with Al_2O_3 were assigned as the active sites for the dehydrogenation reaction [11–13]. However, the dehydrogenation activity of Ga_2O_3-based catalysts still needs improvements. In addition, it has been reported [14] that the PDH performance of Ga/Al_2O_3 could be remarkably improved through the addition of trace amount of platinum (0.1 wt%) on the catalyst, whereas in absence of Ga_2O_3, the activity of 0.1 wt% Pt/Al_2O_3 is negligible. Thus, Ga_2O_3 is supposed to be the active sites in the dehydrogenation process. Therefore, it is significant to investigate the synergistic function mechanism between the Pt and Ga_2O_3 in the reaction for further improvement of the dehydrogenation performance via rational modification of the structure of the catalyst as well as the deep understanding of Ga_2O_3-catalyzed dehydrogenation mechanism.

In the present work, in order to investigate and further improve the synergistic function between Pt and Ga_2O_3 as well as to profoundly understand the dehydrogenation performance of Ga_2O_3-based catalysts, we tentatively modulated the interaction between Pt and Ga_2O_3 through tuning the coordination structure of Al^{3+} in Al_2O_3 supports through various preparation methods. And the dehydrogenation performance of the Ga_2O_3-based catalysts was evaluated. NMR and TEM were utilized to elucidate the locations of the supported metal ions and the influence of unsaturated coordinate Al^{3+} (Al^{3+}_{penta}) sites on their dispersion. H_2-TPR was also performed to unveil the synergistic effect of Pt

* Corresponding author.
E-mail addresses: yutie043116@dicp.ac.cn, yutie043116@tju.edu.cn (T. Yu).

https://doi.org/10.1016/j.jechem.2019.04.027

and Ga_2O_3 and the hydrogen spillover ability. Finally, the reaction mechanism of propane dehydrogenation over the catalyst was proposed, and their stability was also examined through cycling tests.

2. Experimental

2.1. Catalyst preparation

C–Al_2O_3 used in the present work is commercial Al_2O_3, purchased from Alfa Aesar (1/8 pellets, product # 43832), with a specific surface area of 256 m^2/g. Sg–Al_2O_3 was prepared using a sol-gel method [15]. Briefly, 2.85 g $EO_{20}PO_{70}EO_{20}$ (Aldrich, Pluronic P123, average molecular weight = 5800 g/mol) was dissolved in a mixture of 60 mL ethanol and 4.8 mL concentrated HNO_3 (65–68 wt%) by blending at room temperature. Then 6.12 g aluminum isopropoxide was added into the above solution, which was stirred overnight. The clear solution was then put into an oven and dried at 65 °C for 48 h. The dried gel was grinded to powders and then calcined in static air from room temperature to 550 °C at a ramping rate of 1 °C/min and held for 6 h, and then elevated to 600 °C at 5 °C/min and held for 2 h. Hd–Al_2O_3 was synthesized via a hydrothermal homogeneous precipitation process [16]. Briefly, 7.5 g $Al(NO_3)_3{\cdot}9H_2O$, 9.61 g urea and 2.96 g L-lysine were dissolved in 65 mL deionized water. The obtained mixture was then transferred into a 100 mL Teflon-lined autoclave, and sealed at 100 °C for 48 h. After this procedure, the precipitates were washed thoroughly with deionized water several times, dried at 110 °C, and then heated to 600 °C at a ramping rate of 2 °C/min and calcined for 4 h.

Ga/C–Al_2O_3 was prepared by a wet impregnation method. Firstly, a certain amount of $Ga(NO_3)_3{\cdot}xH_2O$ was dissolved in deionized water, and then C–Al_2O_3 with a desired amount was added into the above solution. After stirring at room temperature until dry sediment, the product was dried at 110 °C overnight, and then calcined in air at 600 °C for 4 h. Ga/Sg–Al_2O_3 and Ga/Hd–Al_2O_3 were prepared following the same procedure as Ga/C–Al_2O_3.

Pt/Ga/Al_2O_3 was prepared by impregnation of Pt onto different Ga/Al_2O_3. The final products were calcined in air at 600 °C for 4 h. The loading of Pt and Ga was 0.1 wt% and 5 wt%, respectively, for all catalysts.

2.2. Catalytic activity measurements

Reaction was carried out in a quartz tube with an inner diameter of 9 mm, which was packed with 0.10 g catalyst (40–60 mesh pellets). The reaction conditions were 853 K, 10 kPa propane, 90 kPa N_2 with a total flowrate of 20 mL/min. Note that blank experiment confirms the pyrolysis of propane could be neglected at the present reaction conditions. An online gas chromatograph was used to analyze the effluents. For the regeneration, the spent catalysts were regenerated at 600 °C for 30 min in a flowing dry air (20% O_2 in N_2).

2.3. Catalyst characterization

X-ray diffraction (XRD) was carried out on a Rigaku D/Max 2500 diffractometer with a Cu K_α mono-chromatic radiation source from 10° to 80° at a scan rate of 5°/min.

The nitrogen adsorption-desorption isotherms were measured at −196 °C on a Micromeritics ASAP 2020 apparatus. Prior to the measurements, the samples were degassed at 300 °C for 4 h. The specific surface area of the samples was determined by the Brunauer–Emmett–Teller (BET) method. The cumulative pore volume and pore size were calculated from the desorption branches of the isotherms employing the Barrett–Joyner–Halenda (BJH) method.

Temperature programmed reduction by H_2 (H_2-TPR) was carried out on a Micromeritics Auto Chem II 2920 system. Prior to the TPR characterization, the catalysts (100 mg) were dried in flowing Ar at 200 °C for 1 h. A 10% (v/v) H_2 in Ar mixture was used as the reductant with a flow rate of 25 mL/min. The TPR profile was recorded while the catalyst was heated at a rate of 10 °C/min up to 700 °C. STEM and EDX-mapping images were taken with JEM-2100F at an accelerating voltage of 200 kV.

The NMR experiments were carried out on Bruker Avance III 600 spectrometers (14.1 T) using 4 mm wvt probe with the spinning rate of 13.0 kHz at ambient temperature. ^{27}Al and ^{71}Ga experiments were carried out at 156.37 and 183.01 MHz, respectively. ^{27}Al MAS NMR studies were performed with a pulse length of 0.73 μs, a recycle delay of 0.5 s with 1024 accumulations. ^{71}Ga MAS NMR spectra were recorded with a pulse length of 2.0 μs, a recycle delay of 2 s with 1024 accumulations. ^{27}Al and ^{71}Ga NMR spectra were referenced using $(NH_4)Al(SO_4)_2{\cdot}12H_2O$ ($\delta(^{27}Al) = -0.4$ ppm) and $Ga(NO_3)_3$ ($\delta(^{71}Ga) = 0$ ppm), respectively.

XPS experiments were performed on a Thermofisher ESCALAB 250Xi instrument, equipped with an Al K_α (1486.6 eV) X-ray anode. The binding energies were calibrated using C1*s* peak of contaminant carbon (BE = 284.6 eV).

3. Results and discussion

3.1. Catalytic performance

The catalytic activities of various Ga/Al_2O_3 catalysts prepared via different methods are displayed in Fig. 1. It is seen that Ga/C–Al_2O_3 exhibits the best catalytic activity, with the propane conversion decreasing from 19.7% to 14.2% after 3 h time on stream. The dehydrogenation activity of Ga/Hd–Al_2O_3 is inferior to Ga/C–Al_2O_3, whereas its stability is better. Ga/Sg–Al_2O_3 shows the lowest activity among them. Their selectivity for C_3H_6 follows the same sequence as the catalytic activity, and Ga/C–Al_2O_3 displays the highest selectivity (>90%).

After a trace amount of platinum loading onto the Ga/Al_2O_3 catalysts, the dehydrogenation performance of all catalysts shows an abrupt enhancement compared to their parent counterparts without Pt in Fig. 2. Moreover, Pt/Ga/Hd–Al_2O_3 and Pt/Ga/Sg–Al_2O_3 present much more activity increment in comparison with Pt/Ga/C–Al_2O_3. For instance, the initial conversion of propane is 65.5%, 59.0%, and 36.7% for Pt/Ga/Hd–Al_2O_3, Pt/Ga/Sg–Al_2O_3, and Pt/Ga/C–Al_2O_3, whereas they are only 11.5%, 8.0%, and 19.6% in the absence of Pt. It is worth to note that the PDH activity of Pt/Hd–Al_2O_3 and Pt/Sg–Al_2O_3 could be neglected under the present conditions (Fig. S1). The conversion of propane on Pt/C–Al_2O_3 is slightly higher than that on the other two catalysts.

In addition, the comparison of dehydrogenation performance over the Pt/Al_2O_3, Ga/Al_2O_3 and Pt/Ga/Al_2O_3 catalysts illustrates the promoting effect of Pt and the vital role of Ga/Al_2O_3 structure on the PDH activity. Moreover, the synergistic effect between Pt and Ga_2O_3 improves the activity of Pt/Ga/Hd–Al_2O_3 and Pt/Ga/Sg–Al_2O_3 much more significantly than Pt/Ga/C–Al_2O_3.

The structure of Ga/Hd–Al_2O_3 and Ga/Sg–Al_2O_3 is also beneficial for a high selectivity of C_3H_6 in the presence of Pt and it remains above 95% over Pt/Ga/Hd–Al_2O_3 and Pt/Ga/Sg–Al_2O_3 throughout the 200 min. In comparison, the initial selectivity of C_3H_6 is 95.5% over Pt/Ga/C–Al_2O_3, and it decreases to 92.2% after 3 h, which is similar to the propene selectivity on the bare Ga/C–Al_2O_3. With time on stream, however, these catalysts deactivated gradually.

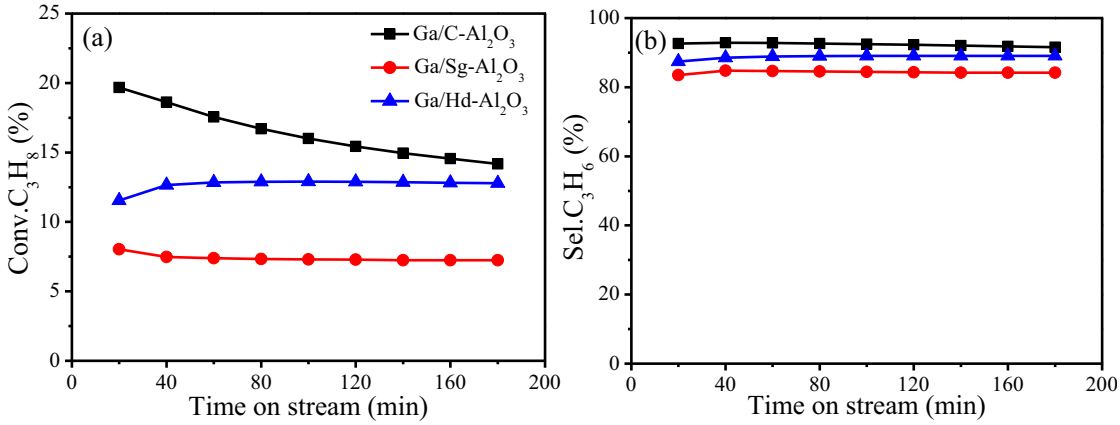

Fig. 1. Propane conversion (a) and propylene selectivity (b) as a function of reaction time for different Ga/Al_2O_3 catalysts.

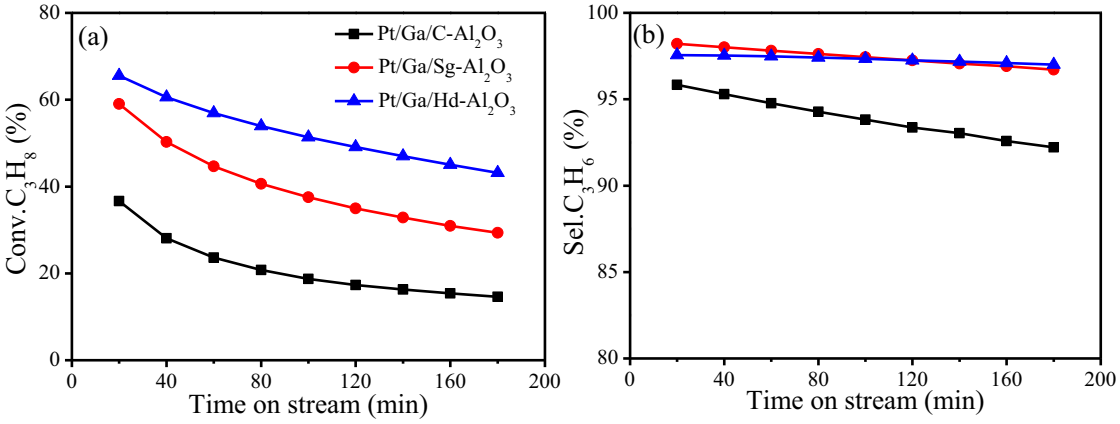

Fig. 2. Propane conversion (a) and propylene selectivity (b) as a function of reaction time for different $Pt/Ga/Al_2O_3$ catalysts.

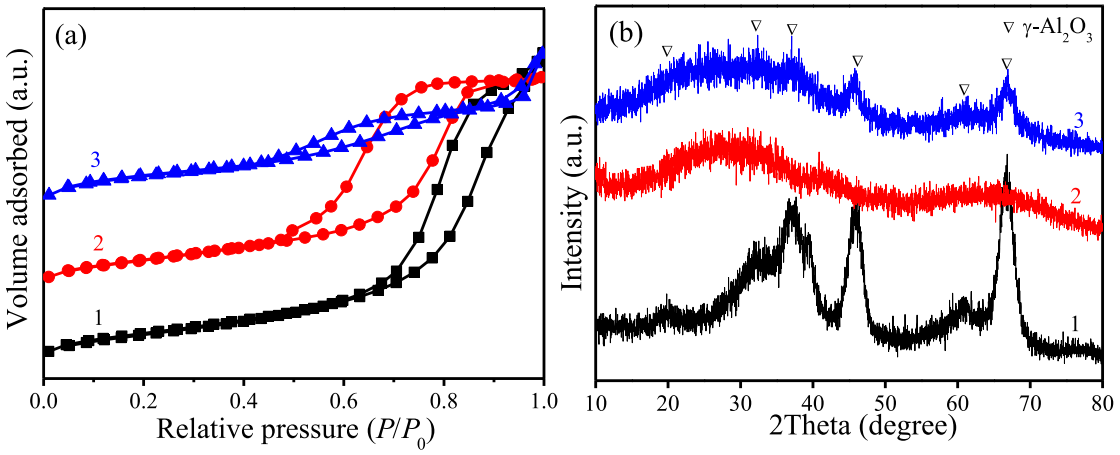

Fig. 3. N_2 adsorption–desorption isotherm (a) and XRD spectra of the synthesized Ga/Al_2O_3 samples (b): (1) $Ga/C–Al_2O_3$; (2) $Ga/Sg–Al_2O_3$, (3) $Ga/Hd–Al_2O_3$.

3.2. Structure and properties of the catalysts

The PDH activity of different platinum-promoted Ga/Al_2O_3 catalysts differentiates greatly. To understand this difference, the structure and property of these catalysts were characterized and analyzed as following. Table S1 lists the basic textural data of different Ga/Al_2O_3 catalysts. The BET surface area of $Ga/C–Al_2O_3$ and $Ga/Sg–Al_2O_3$ is similar, and that of $Ga/Hd–Al_2O_3$ becomes slightly higher. In addition, the isotherms of N_2 adsorption-desorption (Fig. 3a) for all catalysts exhibit the IV type, indicating the mesoporous structure of all Ga/Al_2O_3 samples.

The XRD spectra are presented in Fig. 3(b). $Ga/C–Al_2O_3$ and $Ga/Hd–Al_2O_3$ exhibit the characteristic diffraction patterns of γ-Al_2O_3. The much weaker diffraction of $Ga/Hd–Al_2O_3$ than that of $Ga/C–Al_2O_3$ indicates the poor crystallinity of Al_2O_3 in $Ga/Hd–Al_2O_3$. On the other hand, $Ga/Sg–Al_2O_3$ shows a diffraction peak around 22° as well as a broad diffraction peak at 67° indexed as (440) diffraction of γ-Al_2O_3. The XRD patterns of the samples indicate that there is a mixture of amorphous and γ-Al_2O_3 phase in $Ga/Sg–Al_2O_3$ and $Ga/Hd–Al_2O_3$. No diffraction peaks of Ga_2O_3 are observed, indicating that Ga_2O_3 is highly dispersed and/or due to its low loading.

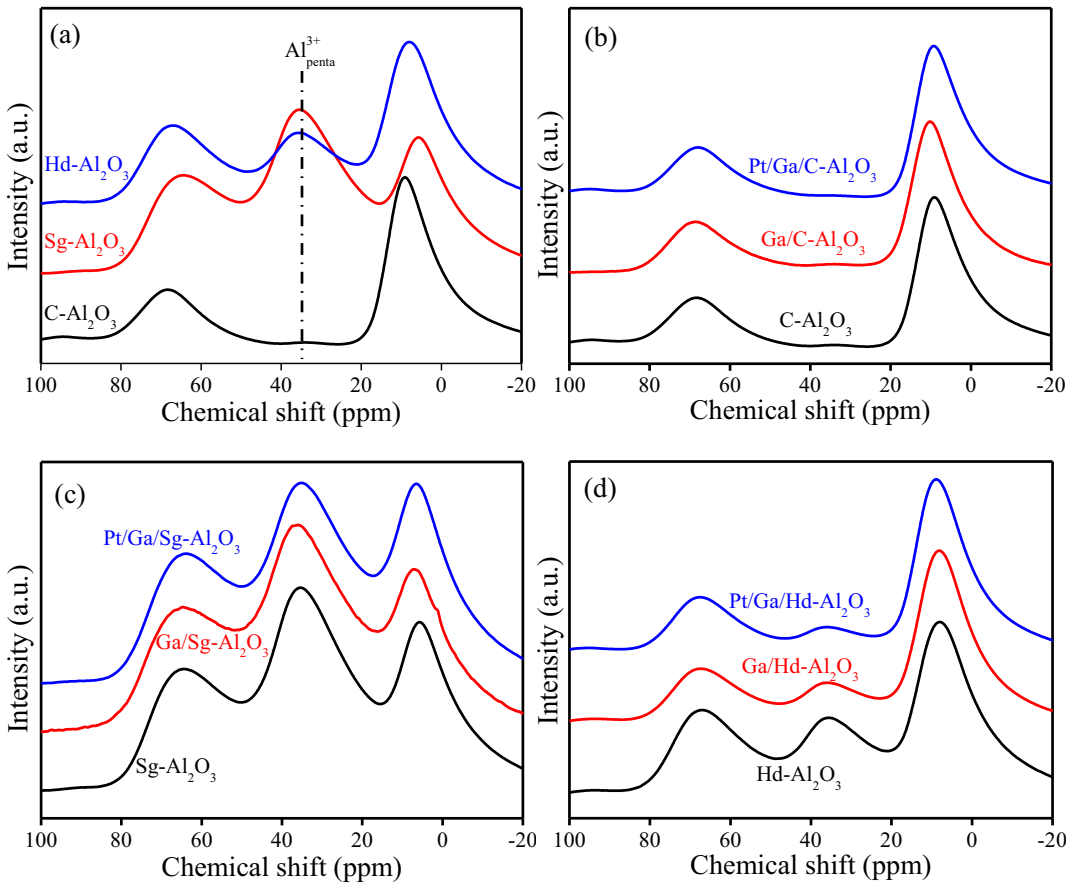

Fig. 4. ^{27}Al MAS NMR spectra of the synthesized Al_2O_3, Ga/Al_2O_3 and $Pt/Ga/Al_2O_3$ samples.

The differences in crystallinity and phases of Al_2O_3 in Ga/Al_2O_3 reflect the different coordination structures of Al^{3+}, which could influence the dispersion of loaded species as well as the metal-support interaction, and thereby leading to different catalytic behavior. MAS NMR characterization gives detailed information about the coordination structure of Ga^{3+} and Al^{3+} in the catalysts. The ^{71}Ga MAS-NMR spectra of Ga/Al_2O_3 and $Pt/Ga/Al_2O_3$ samples are shown in Fig. S2(A, B). There is no visible peak for ^{71}Ga in $Ga/C–Al_2O_3$, indicating that the Ga^{3+} ions are in a very low symmetry that causes a very strong electric field gradient at the location of the nuclei [17]. The NMR peak at 0 ppm in $Ga/Sg–Al_2O_3$ and $Ga/Hd–Al_2O_3$ indicates that Ga^{3+} is octahedral-coordinated in these two samples [18]. After the trace amount of Pt loading, however, there is no ^{71}Ga peak for all $Pt/Ga/Al_2O_3$ catalysts, indicating the asymmetric coordination environment of Ga^{3+} ions in the catalysts. There have been studies [19–21] about the effect of Ga^{3+} coordinate structure on the Lewis acidity as well as the catalytic dehydrogenation property. It is shown that different Ga^{3+} coordinate structures almost presented less impact on catalytic activity of Ga_2O_3 than other factors.

The ^{27}Al MAS-NMR spectra of Al_2O_3, Ga/Al_2O_3 and $Pt/Ga/Al_2O_3$ samples are displayed in Fig. 4. $C–Al_2O_3$ exhibits two peaks at 10 and 68 ppm (Fig. 4a) representing Al^{3+} ions in octahedral (Al^{3+}_{octa}) and tetrahedral (Al^{3+}_{tetra}) coordination, respectively, which is the characteristic ^{27}Al NMR features of γ-Al_2O_3. Besides, there is also a rather weak NMR peak at 35 ppm, which is assigned to Al^{3+} ions in unsaturated pentahedral coordination (Al^{3+}_{penta}) [22,23]. Importantly, as for $Sg–Al_2O_3$ and $Hd–Al_2O_3$, besides Al^{3+}_{octa} and Al^{3+}_{tetra}, there is a considerable content of Al^{3+}_{penta}. It is clearly seen that the coordinate structure of Al_2O_3 supports are quite different due to the various preparation methods. Additionally, the slight differences of the chemical shifts of Al^{3+}_{octa} and Al^{3+}_{tetra} are proposed to be due to the different chemical environments in different Al_2O_3 samples.

Table 1. Coordination states of Al^{3+} in different samples.

Samples	Percentage of different coordinated Al^{3+} sites (%)[a]		
	Al^{3+}_{octa}	Al^{3+}_{penta}	Al^{3+}_{tetra}
$C–Al_2O_3$	67.5	3.0	29.5
$Ga/C–Al_2O_3$	70.9	–	29.1
$Pt/Ga/C–Al_2O_3$	70.5	–	29.5
$Sg–Al_2O_3$	24.8	52.1	23.1
$Ga/Sg–Al_2O_3$	31.2	43.3	25.5
$Pt/Ga/Sg–Al_2O_3$	36.3	40.0	24.7
$Hd–Al_2O_3$	47.7	24.9	27.4
$Ga/Hd–Al_2O_3$	55.8	18.8	25.4
$Pt/Ga/Hd–Al_2O_3$	60.2	13.2	26.6

[a] : Notably, the percentages of various coordination states of Al^{3+} are calculated based on the peak areas of different coordinated Al^{3+} sites.

Fig. 4(b)–(d) shows that after the deposition of Ga and Pt, the peak intensity of Al^{3+}_{penta} decreases for all the samples, and concomitantly, the peak intensity at 10 ppm corresponding to Al^{3+}_{octa} increases. The quantification of Al^{3+} ions content in different coordination structures is shown in Table 1. From the data in Fig. 4 and Table 1, it is concluded that the loading of Pt and Ga causes the decrease of Al^{3+}_{penta} sites and the increase of Al^{3+}_{octa} sites at the same time.

The quantification results in Table 1 clearly suggest that the deposited platinum and gallium ions interact preferentially with the

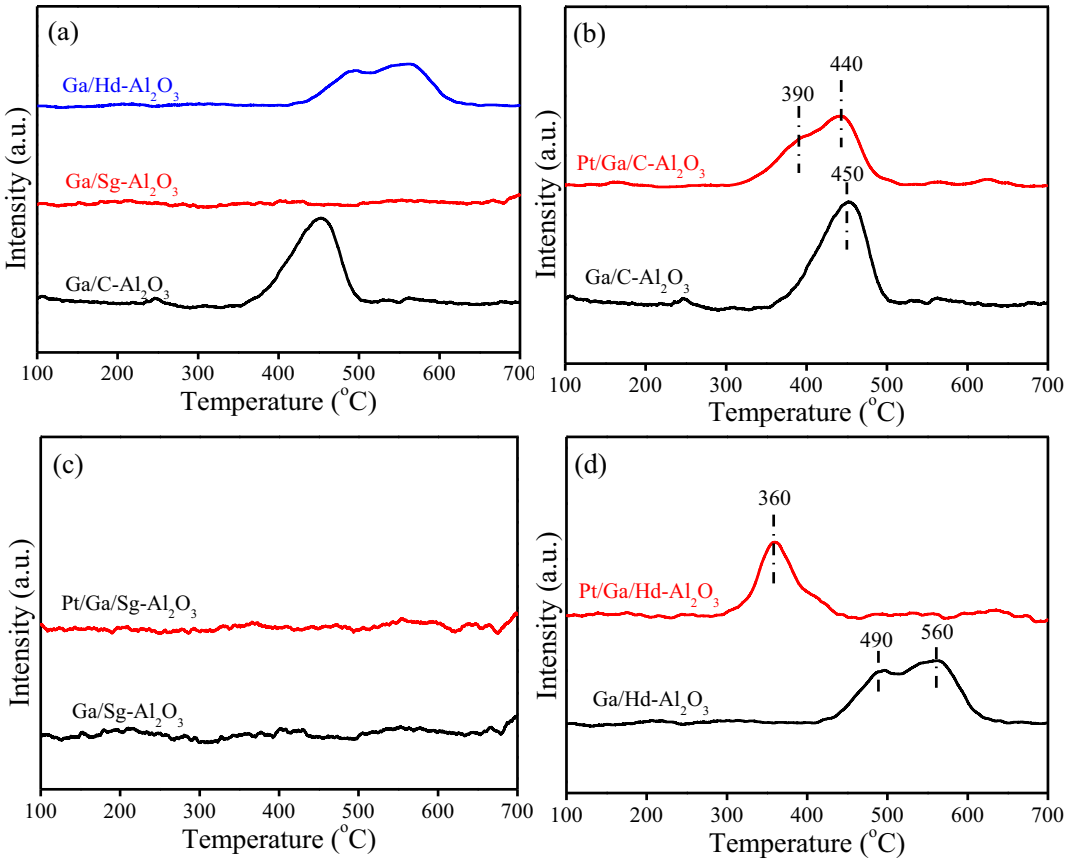

Fig. 5. H_2-TPR profiles of various catalysts.

Al^{3+}_{penta} sites. The unsaturated Al^{3+}_{penta} sites tend to anchor the loaded ions via the oxygen bridge to achieve more stable Al^{3+}_{octa} coordinate state [22,23]. This is likely the reason for the diminished Al^{3+}_{penta} sites and the increased Al^{3+}_{octa} sites upon Ga_2O_3 and Pt loading in Pt/Ga/Hd–Al_2O_3 and Pt/Ga/Sg–Al_2O_3. Thus, the interaction between the dopants and the supports, i.e., the metal-support interaction, might be reinforced through the driving force of the coordinative saturation of the Al^{3+}_{penta} sites.

Since Al^{3+}_{penta} sites have the strong tendency to bind the dopants to achieve the coordination-saturated state, it is reasonable to anticipate that a strong metal-support interaction in the catalysts could be generated on Al_2O_3 support with plenty amount of Al^{3+}_{penta}. The interaction between Ga_2O_3 and Al_2O_3 in the Ga/Al_2O_3 and Pt/Ga/Al_2O_3 samples was investigated by H_2-TPR in Fig. 5. From Fig. 5(a), it is seen that for Ga/Al_2O_3 samples, there is one reduction peak around 450 °C for Ga/C–Al_2O_3, whereas there is a major peak at 560 °C with a shoulder at 490 °C on Ga/Hd–Al_2O_3. For Ga/Sg–Al_2O_3, there is no obvious H_2 consumption peak. The gallium oxide species in Ga/Hd–Al_2O_3 are more difficult to be reduced than that in Ga/C–Al_2O_3, indicating the stronger interaction between Ga_2O_3 and Al_2O_3 in Ga/Hd–Al_2O_3 than Ga/C–Al_2O_3. At the same time, the interaction between Ga_2O_3 and Al_2O_3 in Ga/Sg–Al_2O_3 seems to be the strongest among these three samples. It is already mentioned that the difference of interaction strength between Ga_2O_3 and Al_2O_3 is mainly related with the structures of alumina supports. Sg–Al_2O_3 and Hd–Al_2O_3 with more Al^{3+}_{penta} sites could enhance the stronger binding of Ga^{3+} ions.

The addition of trace amount of Pt onto Ga/Al_2O_3 promotes the reduction of Ga_2O_3 on the catalyst. As shown in Fig. 5(b), for Pt/Ga/C–Al_2O_3, the reduction of Ga_2O_3 displays one peak at 440 °C with a shoulder at 390 °C. Due to the rather low amount of Pt on the catalyst, there is no obvious H_2 consumption peak of PtO_x. Compared to Ga/C–Al_2O_3, the reduction peak of Pt/Ga/Al_2O_3 moves to a lower temperature. The reducibility of Ga_2O_3 might be related with the promoted H_2 spillover by Pt, which was also reported previously for Pt/Ga zeolite system in the aromatization processes of lower alkanes [24,25]. The shoulder peak at the lower temperature (390 °C) demonstrates the more effective hydrogen spillover between the Ga_2O_3 and Pt species. In addition, the reduction profile of Pt/Ga/Hd–Al_2O_3 shows an overall lower reduction temperature than Pt/Ga/C–Al_2O_3, although the reduction of Ga_2O_3 in Ga/Hd–Al_2O_3 is more difficult than Ga/C–Al_2O_3, indicating that the presence of Pt enhances the reduction of Pt/Ga/Hd–Al_2O_3 compared to the other catalysts. As for Pt/Ga/Sg–Al_2O_3, there is still no obvious H_2 consumption peak due to the strong interaction between Ga_2O_3 and Al_2O_3 in Ga/Sg–Al_2O_3. To be noted, the quantification of H_2 consumption reveals that only a small amount of gallium oxides (< 5%) is reduced under the present conditions. The Ga_2O_3 could be reduced to metallic Ga and Ga_2O, which are liquid and volatile under the present conditions, respectively, and thus it is deduced that the real active state of gallium is Ga_2O_3 in PDH.

STEM and EDX-mapping characterizations (Fig. 6) were undertaken to investigate the Pt and Ga dispersion on C–Al_2O_3 and Hd–Al_2O_3. As shown in Fig. 6(a), 5–8 nm Pt particles are clearly observed on the Pt/Ga/C–Al_2O_3 catalyst, even though the loading amount of Pt is only 0.1 wt%. The EDX mapping images show that Pt particles prefer to deposit around Ga_2O_3 sites, and it is clearly seen that the distribution of Ga_2O_3 and Pt species is not uniform on Al_2O_3.

On the other hand, as shown in Fig. 6(b), there is no discernable Pt particles in Pt/Ga/Hd–Al_2O_3, and the EDX-mapping results show that Pt, Ga, and Al elements distribute very homogeneously,

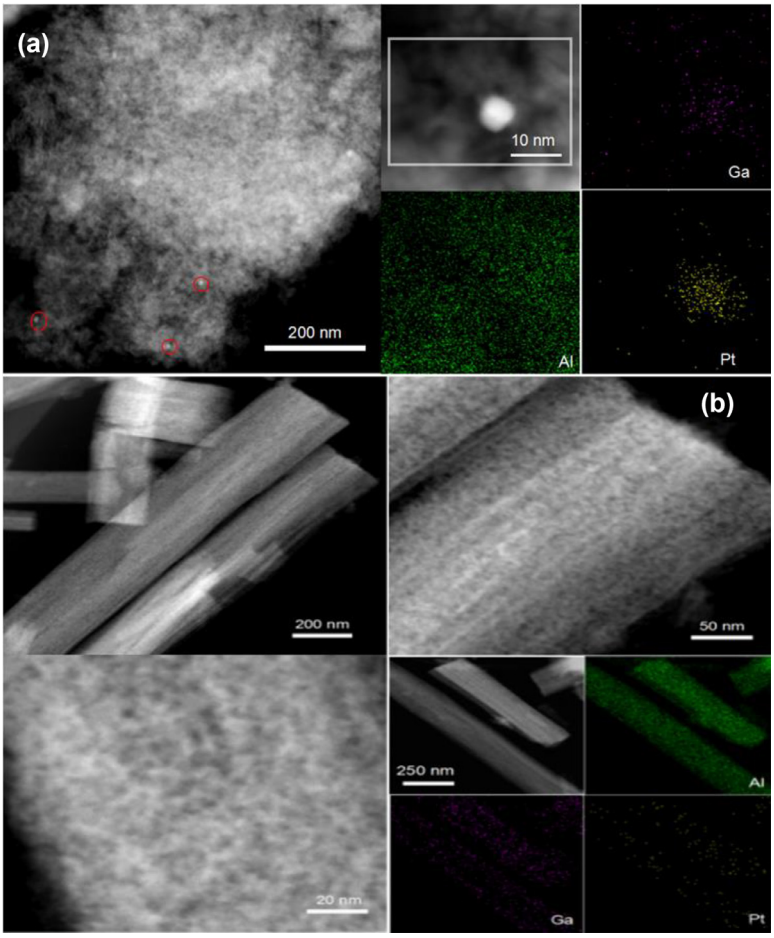

Fig. 6. STEM-EDX-mapping photographs of Pt/Ga/C–Al_2O_3 (a) and Pt/Ga/Hd–Al_2O_3 (b) catalysts.

indicating the well dispersion of Pt and Ga_2O_3 on Hd–Al_2O_3. Combining with the MAS NMR characterizations on the Al^{3+} coordination structures, it is reasonably deduced that the considerable amount of $Al^{3+}{}_{penta}$ sites in Hd–Al_2O_3 promote the homogeneous distribution of Pt and Ga via the driving force to achieve the coordinate saturated state. To correlate with the reduction behavior of different catalysts, it is proposed that the well dispersed Pt and Ga on alumina supports promotes hydrogen spillover from supported platium to gallium species, which is anticipated to play an important role in dehydrogenation [26,27].

Herein, to explain the activity differences of various catalysts in Fig. 2, the metal-support interaction and the synergistic function between Pt and Ga_2O_3 via hydrogen spillover are presumably the two main determinants in the dehydrogenation process. Since Pt/Hd–Al_2O_3 (in absence of Ga_2O_3) is almost inactive for the dehydrogenation of propane, Ga_2O_3 is regarded as the active component for dehydrogenation, which was reported previously [8–13]. In addition, wide studies indicated that the rate-determining step for the dehydrogenation of propane is the hydrogen transfer and desorption from the active sites on Ga_2O_3 catalysts [28–30]. The improved hydrogen transportation efficiency is proposed to be the reason for the remarkably enhanced dehydrogenation activity when a trace amount of Pt (1000 ppm) is well dispersed on Ga/Hd–Al_2O_3. The homogeneously dispersed platinum species likely facilitates the hydrogen transfer and desorption from Ga_2O_3 effectively via hydrogen spillover. Thus, the active hydrogenation sites are released for further reaction, which consequently improves the PDH performance of Ga_2O_3. For Ga/Sg–Al_2O_3, even though it contains the largest number of unsaturated $Al^{3+}{}_{penta}$ sites among the prepared Ga/Al_2O_3 samples (Table 1), it is suggested that the too strong interaction between Ga and $Al^{3+}{}_{penta}$ sites in Ga/Sg–Al_2O_3 (Fig. 5) may affect the activation of propane and hence limiting the activity of Pt/Ga/Sg–Al_2O_3 for PDH, as shown in Fig. 2. Due to the least unsaturated $Al^{3+}{}_{penta}$ sites and nonuniform platinum dispersion, Pt/Ga/C–Al_2O_3 shows the lowest PDH activity.

3.3. Recyclability of the Pt/Ga/Hd–Al_2O_3 catalyst

As shown in Fig. 2, the PDH activity of the Pt/Ga/Al_2O_3 catalysts declines gradually with time on stream. The catalyst deactivation with time on stream is frequently reported in the direct dehydrogenation reactions. To recover its PDH activity, regeneration of the catalysts is necessary. Therefore, the catalyst's cycling stability is important for its future application. For Pt/Ga/Hd–Al_2O_3 here, after reaction for 2 h at 580 °C, the catalyst is flushed by He for 5 min and then regenerated in dry air at 600 °C for 30 min. The reaction results are displayed in Fig. 7.

The conversion of propane on Pt/Ga/Hd–Al_2O_3 decreases stepwise in the first 3 cycles, and thereafter its activity stabilizes. At the same time, the selectivity of propene presents the same trend with activity. The decrease of PDH performance is probably due to the variation of the structure and/or composition of active sites during the reaction-regeneration processes and does not change further after the third cycle. Thus it is inferred that besides the best PDH activity of Pt/Ga/Hd–Al_2O_3 among the synthesized catalysts, this catalyst also possesses a high recycling stability, which is significant for its future application.

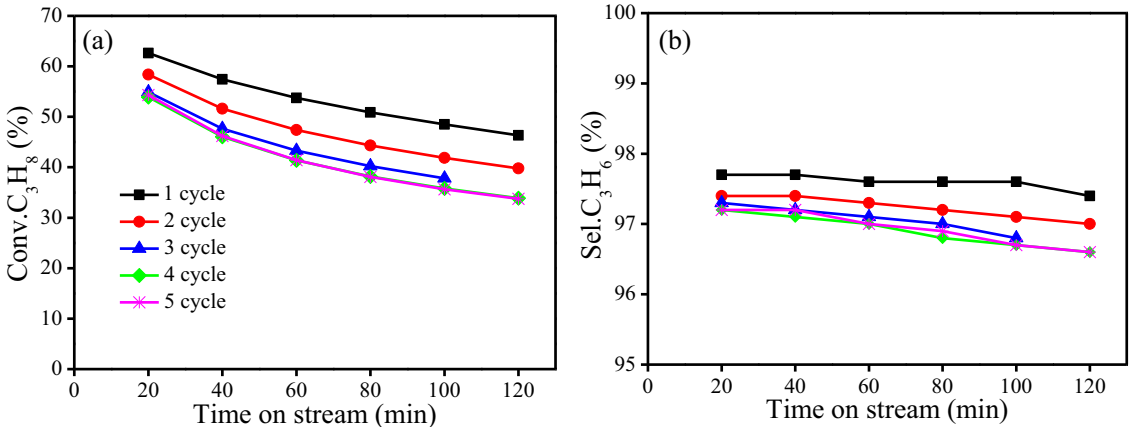

Fig. 7. Stability test of Pt/Ga/Hd–Al_2O_3 by a reaction-regeneration cycle experiment. Propane conversion (a) and propene selectivity (b).

4. Conclusions

The difference of the Al^{3+} coordination structure in Pt/Ga/Al_2O_3 catalysts and the synergistic interaction between platinum and Ga_2O_3 were designed to examine their impact on PDH activity. It was shown that the catalyst containing a considerable content of unsaturated coordinate Al^{3+} sites (penta-coordinated Al^{3+}, Al^{3+}_{penta}) benefited PDH activity. Characterization of the catalysts revealed that Al^{3+}_{penta} sites promoted the dispersion of platinum and gallium ions on the Al_2O_3 support, which facilitated the effective hydrogen spillover between Pt and Ga and generated hydrogen desorption from the active sites of Ga_2O_3. Both of them consequently facilitated the dehydrogenation of propane. Furthermore, the cycling experiments demonstrated that the Pt/Ga/Hd–Al_2O_3 catalyst exhibited a rather good stability as the initial PDH activity dropped by 10% in the first 3 cycles and then stabilized.

Acknowledgments

The authors are grateful to the National Natural Science Foundation of China (No. 21676195) and the China Postdoctoral Science Foundation (2016M601347).

Supplementary materials

Supplementary material associated with this article can be found, in the online version, at doi:10.1016/j.jechem.2019.04.027.

References

[1] J.J.H.B. Sattler, J. Ruiz-Martinez, E. Santillan-Jimenez, B.M. Weckhuysen, Chem. Rev. 114 (2014) 10613–10653.
[2] S.A. Bocanegra, A. Guerrero-Ruiz, S.R. de Miguel, O.A. Scelza, Appl. Catal. A 277 (2004) 11–22.
[3] R.D. Cortright, J.A. Dumesic, J. Catal. 148 (1994) 771–778.
[4] C. Sun, Y. Luo, M. Cao, J. Energy Chem. 27 (2018) 311–318.
[5] M.M. Bhasin, J.H. McCain, B.V. Vora, T. Imai, P.R. Pudado, Appl. Catal. A 221 (2001) 397–419.
[6] U. Olsbye, A. Virnovskaia, O. Prytz, S.J. Tinnemans, B.M. Weckhuysen, Catal. Lett. 103 (2005) 143–148.
[7] D. Fang, J. Zhao, W. Li, J. Energy Chem. 24 (2015) 101–107.
[8] B. Zheng, W. Hua, Y. Yue, Z. Gao, J. Catal. 232 (2005) 143–151.
[9] N.S. Nesterenko, O.A. Ponomoreva, V.V. Yuschenko, I.I. Ivanova, F. Testa, Appl. Catal. A 254 (2003) 261–272.
[10] M. Chen, J. Xu, Y. Liu, Y. Cao, H. He, J. Zhuang, K. Fan, Catal. Lett. 124 (2008) 369–375.
[11] Y. Zhang, W. Yao, H. Fang, A. Hu, Z. Huang, Sci. Bull. 60 (2015) 1316–1331.
[12] C. Coperet, Chem. Rev. 110 (2010) 656–680.
[13] M. Chen, J. Xu, F. Su, Y. Liu, Y. Cao, H. He, K. Fan, J. Catal. 256 (2008) 293–300.
[14] J.J.H.B. Sattler, I.D. Gonzalez-Jimenez, L. Luo, B.A. Stears, A. Malek, D.G. Barton, B.A. Kilos, M.P. Kaminsky, T.W.G.M. Verhoeven, E.J. Koers, M. Baldus, B.M. Weckhuysen, Angew. Chem. Int. Ed. 53 (2014) 9251–9256.
[15] Q. Yuan, A. Yin, C. Luo, L. Sun, Y. Zhang, W. Duan, H. Liu, C. Yan, J. Am. Chem. Soc. 130 (2008) 3465–3472.
[16] J. Wang, A. Lu, M. Li, W. Zhang, Y. Chen, D. Tian, W. Li, ACS Nano 7 (2013) 4902–4910.
[17] R. Klik, V. Bosacek, L. Kubelkova, D. Freude, D. Michel, Zeolites 19 (1997) 343–348.
[18] A. Merrouche, J. Patarin, H. Kessler, M. Soulard, L. Delmotte, J.L. Guth, J.F. Joly, Zeolites 12 (1992) 226–232.
[19] A.B. Getsoian, U. Das, J. Camacho-Bunquin, G. Zhang, J.R. Gallagher, B. Hu, S. Cheah, J.A. Schaidle, D.A. Ruddy, J.E. Hensley, T.R. Krause, L.A. Curtiss, J.T. Miller, A.S. Hock, Catal. Sci. Technol. 6 (2016) 6339–6353.
[20] A.A. Gabrienko, S.S. Arzumanov, A.V. Toktarev, A.G. Stepanov, Chem. Phys. Lett. 496 (2010) 148–151.
[21] J.C. Lavalley, M. Daturi, V. Montouillout, G. Clet, C. Otero Arean, M. Rodriguez Delgado, A. Sahibed-dine, Phys. Chem. Chem. Phys. 5 (2003) 1301–1305.
[22] J.H. Kwak, J.Z. Hu, D.H. Kim, J. Szanyi, C.H.F. Peden, J. Catal. 251 (2007) 189–194.
[23] J.H. Kwak, J. Hu, D. Mei, C. Yi, D.H. Kim, C.H.F. Peden, L.F. Allard, J. Szanyi, Science 325 (2009) 1670–1673.
[24] E.S. Shipiro, D.P. Shevchenko, E.V. Dmitriev, O.P. Tkachenko, K.M. Minachev, Appl. Catal. A: Gen. 107 (1994) 165–180.
[25] S. Todorova, B. Su, Catal. Today 93–94 (2004) 417–424.
[26] R. Prins, Chem. Rev. 112 (2012) 2714–2738.
[27] Y. Liu, Z.H. Li, J. Lu, K. Fan, J. Phys. Chem. C 112 (2008) 20382–20392.
[28] Y. Pan, D. Mei, C. Liu, Q. Ge, J. Phys. Chem. C 115 (2011) 10140–10146.
[29] B. Xu, B. Zheng, W. Hua, Y. Yue, Z. Gao, J. Catal. 239 (2006) 470–477.
[30] J. Im, H. Shin, H. Jang, H. Kim, M. Choi, Nat. Commun. doi:10.1038/ncomms4370.